Eur. Phys. J. D (2021) 75:15
https://doi.org/10.1140/epjd/s10053-020-00036-w

THE EUROPEAN PHYSICAL JOURNAL D

Regular Article - Clusters and Nanostructures

Chirality of small niobium clusters

D. C. Navarro-Ibarra[1] and R. A. Guirado-López[2,a]

[1] Departamento de Ciencias Exactas y Tecnología, Centro Universitario de los Lagos, Universidad de Guadalajara, Enrique Díaz de León, 1144, Lagos de Moreno, Jalisco, Mexico
[2] Instituto de Física "Manuel Sandoval Vallarta", Universidad Autónoma de San Luis Potosí, Álvaro Obregón 64, San Luis Potosí 78000, Mexico

Received 26 August 2020 / Accepted 18 December 2020 / Published online 12 January 2021

Abstract. We report on time-dependent density functional theory calculations to study the chiroptical properties of small Nb_9 clusters and their corresponding van der Waals Nb_9Ar_n complexes. The three most stable 9-atom structures considered in the literature are analyzed, and we obtain their lowest-energy atomic configurations, UV–Vis response, and for the first time, the electronic circular dichroism (ECD) spectra of the systems. Excitation energies, as well as oscillator and rotational strengths are calculated using the M06 exchange-correlation functional together with a mixed basis approach where all electron DGDZVP and Def2SV basis are employed for Nb and Ar atoms, respectively. In all cases, the UV–Vis spectra look very similar and are characterized by the formation of a main absorption maxima located at $\sim$ 240 nm; however, the distribution of simulated ECD signals strongly depends on the geometrical structure of the clusters. Our calculated ECD bands show precise features that cover the experimentally accessible 200–300 nm range and extend near the visible part of the spectra, a fact that allows us to distinguish between different niobium cluster geometries. However, weighted averages of calculated ECD spectra for different Nb_9 clusters reveal that isomerization effects might lead to a notable increase/reduction in the intensity of CD lines since the simulated bands could add or cancel each other.

1 Introduction

Elucidating the geometrical structure of small transition metal (TM) clusters has been the subject of intense investigations in the last decades [1–4]. The precise knowledge of the atomic configuration in these small systems is of crucial importance to better understand their physicochemical behavior and spectroscopic properties observed on a macroscopic scale [5–8]. To achieve this goal, a huge amount of experimental studies has been reported mainly employing far infrared [9–12] and photoelectron spectroscopies [13–15]. In addition, mobility measurements [16,17], reaction kinetics [18–20], saturation and desorption studies [21,22], as well as electron diffraction of trapped clusters [23,24] have revealed interesting information about the size and surface structure of such small objects. Finally, optical absorption spectra [12,25,26] and ionization potentials [27,28] have been also measured to analyze the changes in the electronic structure of the clusters when varying their size and chemical composition,

It is important to underline that, in most of the cases, the interpretation of the measured data is difficult to obtain since experimental observations typically correspond to a complex average of different cluster isomers present in the samples. This is clearly illustrated in the case of small Nb_9, Nb_{12}, and Nb_{12}^+ clusters which have been found to react with small gaseous molecules following a bi-exponential behavior [20]. Similar conclusions were obtained in Ref. [29] where far-infrared vibrational resonance enhanced multiple photon dissociation (FIR-MPD) measurements on van der Waals Nb_9Ar_n complexes were reported. In that work, the authors observed variations in the IR signals for different values of the argon atoms n surrounding the clusters, a behavior attributed to the presence of two structural isomers for Nb_9. However, the atomic arrays of these different cluster conformations remain controversial. We must emphasize that niobium is particularly important to analyze since it has demonstrated to possess interesting properties that could have important implications not only for basic science but also for technological applications. For example, in its pure bulk form, Nb is paramagnetic and becomes a superconductor material when cooled below 9.25 K [30]. In addition, it shows high reactivity toward various nonmetal atoms, easily forming for example niobium nitride and niobium carbide materials, extensively employed in the steel industry [31]. It is resistant to corrosion and, as an

Supplementary information The online version of this article (https://doi.org/10.1140/epjd/s10053-020-00036-w) contains supplementary information, which is available to authorized users.

[a] e-mail: guirado@ifisica.uaslp.mx (corresponding author)

oxide, it has been used in several applications such as solar cells, gas sensors, lithium batteries, and catalytic matrices [32]. It is thus reasonable to expect that, in the form of nanostructures or small clusters, interesting novel properties could be obtained.

Clearly, the experimental findings mentioned above have aroused the interest of theoreticians who have developed and applied various methodologies with different levels of approximation to analyze the structural, electronic, and spectroscopic properties of several model niobium clusters of different sizes and varied chemical composition [13,29,33–35]. Among all the theoretical strategies employed, density functional theory (DFT) and its time-dependent implementation (TD-DFT) have been the most popular in the literature, not only for being able to explain with high accuracy the measured data but also due to its well-known capability to predict new phenomena. Despite the abovementioned success of DFT, the atomic configuration of these small TM sub-nanometer-sized systems is still under debate and we consider that additional spectroscopic data are required for a more precise determination of the actual niobium cluster isomers present in real samples.

In this respect, we believe that optical spectroscopy could be very helpful since the optical response of a cluster is strongly correlated to both his geometrical and electronic structures. In particular, electronic circular dichroism (ECD) spectra is one of the most important experimental tools employed to study the structure of a wide range of nano-systems [36]. As is well known, ECD detects small differences in the UV–Vis spectra between right and left circularly polarized light and has been widely applied to analyze, just to mention a few examples, the molecular conformations of TM complexes like, *i*) $[M(1,2\text{-bis[diethylphosphino]ethane})_2]X_2$, where M=Pt(II), Pd(II), or Ni(II) and X = PF_6^- or ClO_4^-, [37] *ii)* for $[Co(trimethylenediamine)_3]^{3+}$, $[Co(acetylacetonato)_3]$, $[Co(ethylenediamine)_2(CN)_2]^+$, and $[Rh(ethylenediamine)_3]^{3+}$ structures, [38] as well as *iv)* for $(+)\text{-}Fe_2[Nb(CN)_8](4\text{-bromopyridine})_8 \cdot 2H_2O$ complexes [39]. We must emphasize that, upon optical stimulation, the niobium-containing coordination compound $(+)\text{-}Fe_2[Nb(CN)_8](4\text{-bromopyridine})_8 \cdot 2H_2O$ has demonstrated to possess the ability to switch the polarization plane of light by 90 degrees. Furthermore, its magnetic properties can be reversibly switched by irradiating with blue and red light, revealing thus that a precise optical control of the material properties can be achieved. Chiral metallic and semiconductor nanoparticles (in both bare and functionalized forms) have been also extensively studied, while nanorods, nanowires, and more complex nano-helices have revealed interesting chiroptical properties [36].

On the contrary, ECD spectra of small isolated Nb clusters have not been reported in the literature. However, we would like to underline the work of Robbins and Thomson [40] where the magnetic circular dichroism (MCD) spectra of octahedral $[Nb_6Cl_{12}]^{n+}$ ($n = 2$–4) clusters has been measured in solution at room temperature. Even if the origin of the MCD spectral features are totally different than the ones explaining Cotton signals in ECD, the authors were able to measure well-defined CD spectral features that depend on the chemical nature of the solvent and, with the help of DFT calculations, report a precise identification of the orbital nature of several of its electronic transitions. In this work, we present thus a preliminary TD-DFT estimation of the ECD spectra for small Nb_9 clusters and their corresponding van der Waals Nb_9Ar_n ($n = 0$–4) complexes. The formers are important to study since, as mentioned in the previous paragraphs, there exists a long-standing controversy related to establishing the actual niobium cluster atomic configurations present in gas phase experiments, a problem that has been difficult to solve due, among other factors, to the existence of isomerization effects (a problematic shared in general by small TM cluster systems). We believe that ECD spectroscopy could be very helpful to shed some more light into this problem. The complexation of Nb_9 clusters with argon atoms is also relevant to analyze since the photo dissociation of these weakly bound Nb_mAr_n species has been used to infer the optical properties of bare Nb_n clusters. Here, we consider the three most common 9-atom niobium isomers reported in the literature [29] and reveal that Nb_9Ar_n clusters ($n = 0$–4) can exhibit, in the experimentally accessible 200–1000 nm range, well defined CD bands. In particular, we demonstrate that, in the 200–300 nm domain, the ECD spectra shows multiple Cotton signals whose sign and intensity are very sensitive to the local atomic environment and could be used to distinguish between different niobium cluster geometries.

Even if at the moment there are no experimental studies available to compare our here-reported theoretical predictions, there exist recent developments published in the literature oriented to analyze chirality in the gas phase such as, photoelectron circular dichroism [41], Coulomb explosion [42,43], and microwave three wave mixing [44] that could lead to experimental ECD measurements in these kind of systems. The rest of the paper is organized as follows. In Sect. 2, we discuss the theoretical model used in our study. In Sect. 3, we present the discussion of our results, and finally, in Sect. 4 the summary and conclusions are given.

2 Theoretical modeling

The structural and electronic properties of Nb_9Ar_n ($n = 0$–4) complexes are obtained within DFT approach with the help of the GAUSSIAN09 software [45]. The Kohn–Sham equations are solved using the M06 exchange-correlation potential [46], together with the all electron DGDZVP [47] and Def2SV [48] basis sets for Nb and Ar atoms, respectively, which is a good compromise between computational costs and accuracy. The three most stable Nb_9 clusters reported in the literature are considered, namely *i*) Nb atoms forming a nonplanar hexagonal array (iso1, C_2), *ii)* arranged in

a triply capped trigonal prism (iso2, C_2) and, *iii)* as a distorted triply capped octahedron (iso3, C_s). In a second step, the previous clusters will be surrounded by nAr atoms, with $n = 0$–4, to simulate the structure of Nb_9Ar_n complexes synthesized in Ref. [29]. We must emphasize that it is not the purpose of the present work to perform an extensive search of the lowest energy atomic configuration but instead to try to reveal general tendencies of the optical properties as a function of the local atomic environment. In all cases, fully unconstrained spin-polarized structural optimizations using the conjugate gradient method are performed. Vibrational frequencies are calculated by diagonalization of the full Hessian matrix within the harmonic approximation [49]. This procedure generates all vibrational modes of our Nb_9Ar_n (n = 0–4) clusters under consideration, that will be of fundamental importance to ensure the stability of the niobium complexes.

The UV–Vis spectra of the argon-containing Nb_9 clusters is obtained from time-dependent DFT calculations at the same M06/ DGDZVP(Nb)/Def2SV(Ar) level of theory. In addition, electronic circular dichroism (ECD) spectra of Nb_9Ar_n (n = 0–4) complexes can be simulated using the approach presented in Ref. [50] where the CD Cotton effect is approximated following the Gaussian curve methodology and the rotational strength can be calculated using our here-considered TD-DFT scheme. Finally, we consider the first 1850 lowest energy electronic excitations, which allow us to cover both the infrared and ultraviolet regions easily accessible to spectrometers.

In order to test the accuracy of the here-considered theoretical methodology, we have performed some test calculations on Nb_2 and Nb_3 clusters for which several experimental studies are available. For the Nb_2 dimer, we obtain a spin multiplicity of 3 as the lowest energy electronic configuration together with a Nb–Nb bond length of 2.14 Å, the latter being in very good agreement with the experimental data of 2.078 Å [51]. We calculate values of 4.3 eV and 468.8 cm^{-1} for the dissociation energy and vibrational frequency of the Nb_2 dimer, respectively, which are of the order of the measured ones namely, 5.24 ± 0.26 eV [52] and 424.9 cm^{-1} [51]. We also find a value of 6.2 eV for the single ionization energy, in excellent agreement with the experimental data of 6.20 ± 0.05 eV [53]. Finally, for the lowest energy Nb_3 trimer (which corresponds to an equilateral triangle) we obtain vibrational frequencies of 201 (double degenerate) and 368.1 cm^{-1}, which are in line with the experimental findings that report values of 227.4 ± 2.9 and 334.9 ± 2.8 cm^{-1} [54]. As expected, the M06 functional has advantages and drawbacks in describing different properties; however, it contains in its definition corrections for medium and long range interactions that we believe are of crucial importance for describing the stability of weakly interacting systems, as well as the UV–Vis and ECD spectra of Nb_9Ar_n clusters. Actually, for the Ar_2 dimer our M06/Def2SV calculations yield values for the equilibrium Ar–Ar bond length of 3.64 Å and a binding energy of 0.03 eV, which are in line with the experimental findings of 3.76 Å and 0.012 eV, respectively [55]. We believe that the previous comparisons give us confidence on the accuracy of our theoretical predictions.

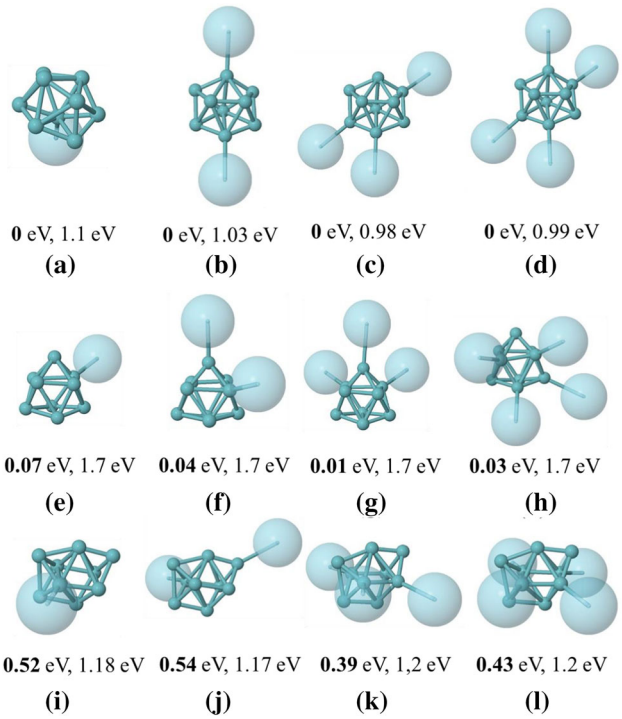

Fig. 1 Optimized atomic configurations for the here-considered model Nb_9Ar_n complexes. The energy difference between lowest energy isomers (first row) with the nearest (second row), and next nearest (third row) cluster structures are specified (bold numbers), together with the value of the HOMO–LUMO energy gap in eV for each case

3 Results and discussion

In Fig. 1, we show the optimized atomic configurations for our here-considered Nb_9Ar_n (n = 1–4) complexes. For each number of surrounding argons and a given Nb_9, isomer several adsorbed configurations for the rare gas atoms on the cluster surface are analyzed; however, in the figure, we only present the lowest energy structures characterized by possessing their lowest spin state. The preferred atomic arrays are shown in Fig. 1a–d and correspond to argon-containing Nb_9 clusters where the TM atoms are found in the form of a nonplanar hexagonal structure (iso1). The energy difference between these configurations with respect to their corresponding closets in energy Nb_9Ar_n (n = 1–4) isomers defined in Fig. 1e–h, where Nb species arrange in a distorted triply capped trigonal prism (iso2), varies in the range of 0.01–0.07 eV (specified in the figure). Furthermore, we obtain that the Nb_9Ar_n complexes presented in Fig. 1i–l, where niobium atoms are organized in a distorted

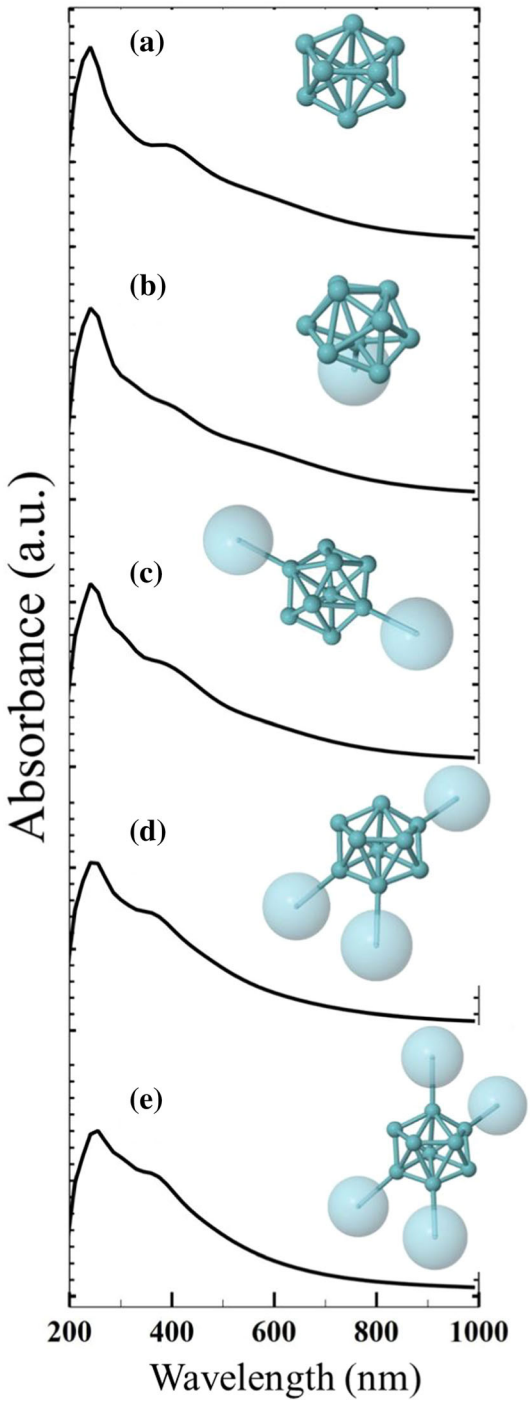

Fig. 2 Simulated UV–Vis spectra for Nb_9Ar_n clusters shown in the first row of Fig. 1 (FWHM = 3000 cm^{-1})

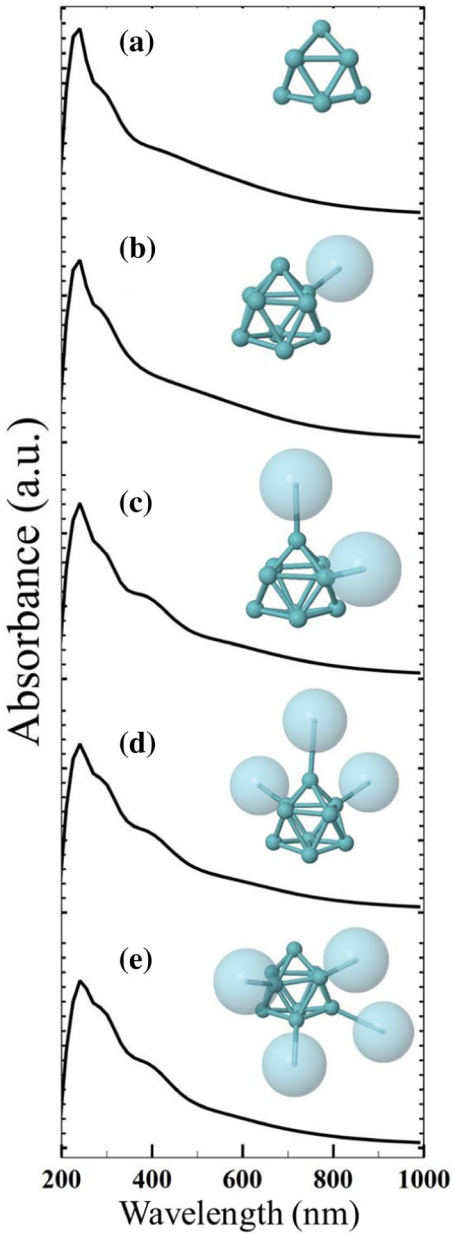

Fig. 3 Simulated UV–Vis spectra for Nb_9Ar_n clusters shown in the second row of Fig. 1 (FWHM = 3000 cm^{-1})

triply capped octahedron (iso3), are the highest energy atomic configurations, being approximately 0.4 eV least stable when compared to the lowest energy structures shown in the first row of Fig. 1. Consequently, and based on total energy arguments, it could be reasonable to expect that in real samples the argon-containing iso3 structures could be the less abundant atomic configurations. In all cases, the argon atoms are weakly adsorbed on Nb_9 clusters, showing different aggregated forms, with Nb–Ar equilibrium distances which vary in the range of 2.86–3.04 Å. As expected, their presence on the surface slightly perturbs the underlying niobium cluster geometries where Nb–Nb nearest neighbor distance variations of approximately 2% (when compared to the bare structures) are found, as well as induces negligible changes in their HOMO–LUMO energy gaps (see Fig. 1). However, when analyzing both the low and high energy side of the spin-polarized electronic spectra (see Figs. S1–S3 of the supporting information) we appreciate variations in the energy level spacing in different regions of the eigenvalue distribution as a function of n,

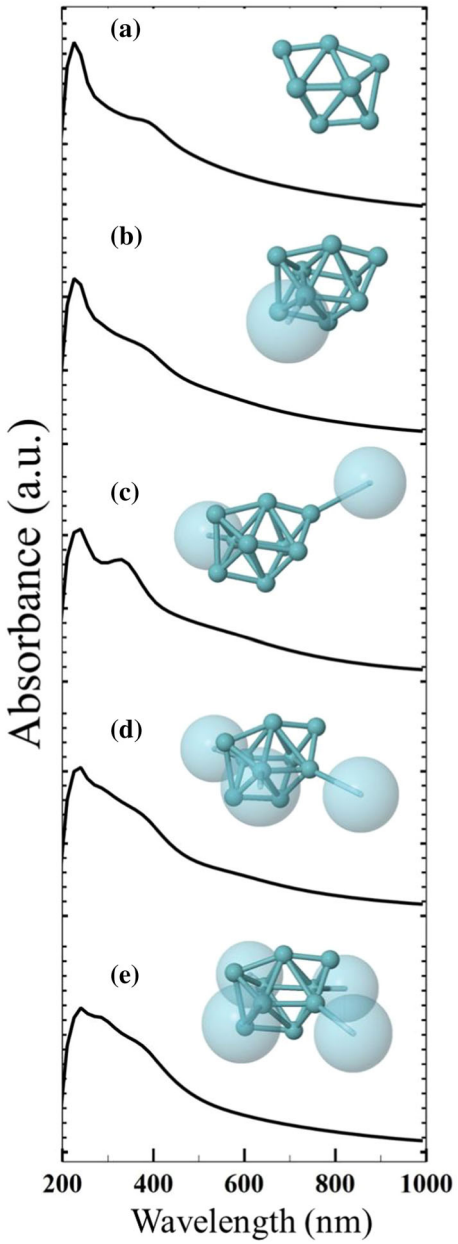

Fig. 4 Simulated UV–Vis spectra for Nb_9Ar_n clusters shown in the third row of Fig. 1 (FWHM = 3000 cm^{-1})

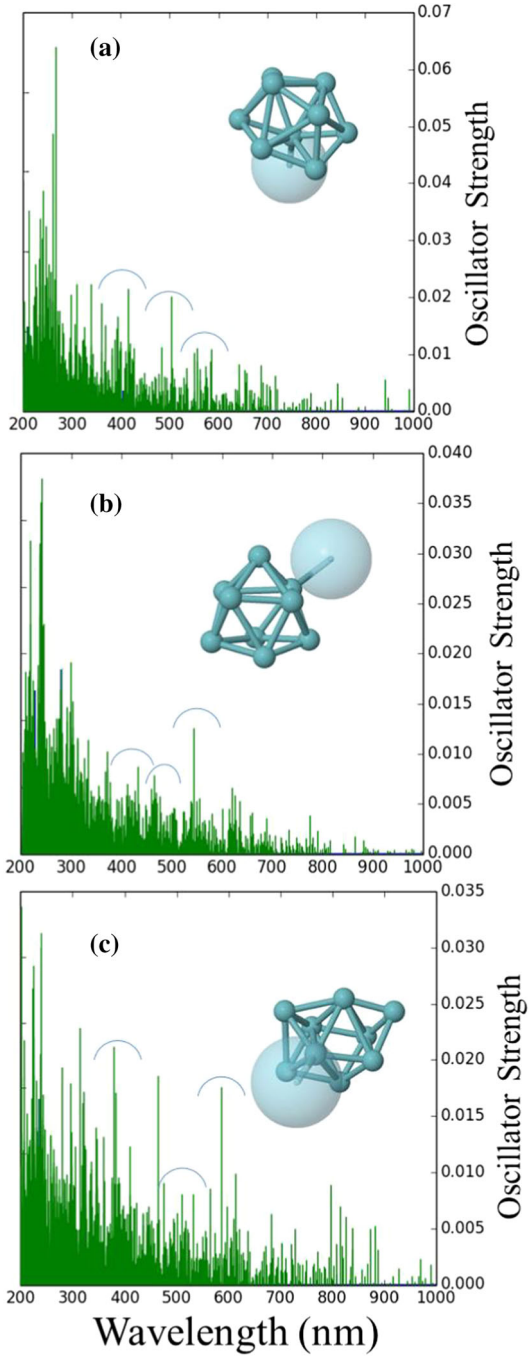

Fig. 5 Distribution of electronic transitions for Nb_9Ar clusters. We include, as a guide to the eye, blue semicircles specifying selected regions of the spectra around 400, 500, and 580 nm where well-defined bands in the experimental spectra are observed

a result that anticipates, as will be seen in the following, small perturbations in the optical absorption behavior.

The results presented in Fig. 1 are in line with the conclusions reported in Ref. [29] where a combined experimental and theoretical (DFT) study analyzing the vibrational properties of the same Nb_9 isomers is reported. In that work, DFT calculations also reveal that the bare iso3 cluster is the less stable atomic array and the authors speculate, based on a direct comparison between simulated and measured infrared vibrational spectra, that a combination of iso1 and iso2 isomers is required to explain their experimental FIR-MPD data. Here, we believe that the previous assumption is also in agreement with our calculations since very small energy differences are found between the corresponding Nb_9Ar, Nb_9Ar_2, Nb_9Ar_3, and Nb_9Ar_4 conformers shown in the first (iso1) and second (iso2) rows of Fig. 1 (0.01–0.07 eV, as specified in the figure). Actually, if reduced interconversion energy barriers between pairs of isomers are additionally obtained, it could be more than reason-

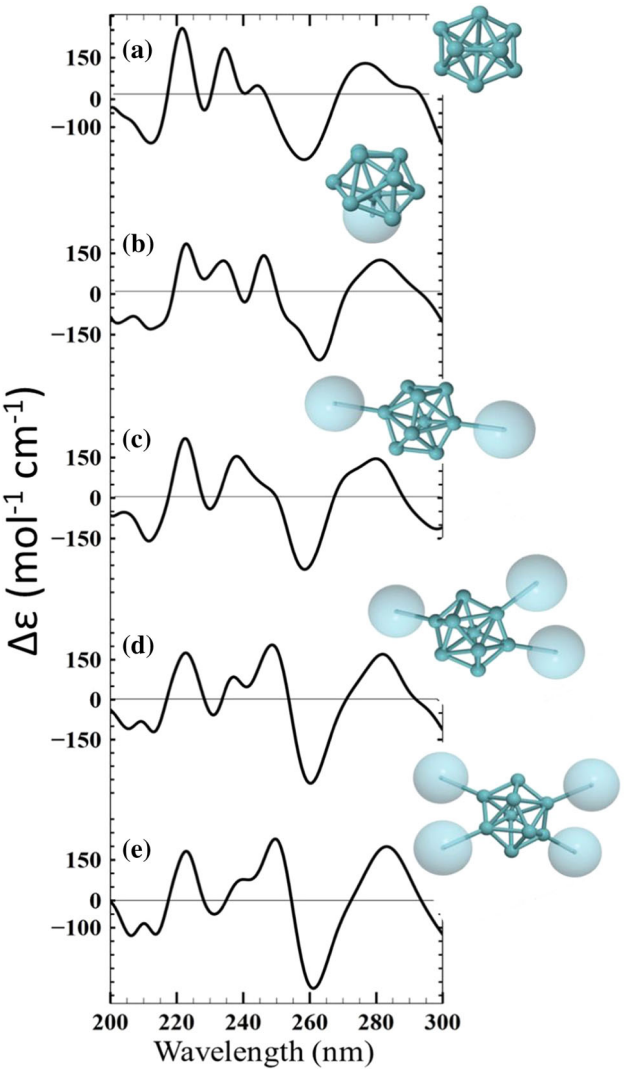

Fig. 6 Simulated ECD spectra for Nb_9Ar_n clusters shown in the first row of Fig. 1 ($\sigma = 0.2$ eV)

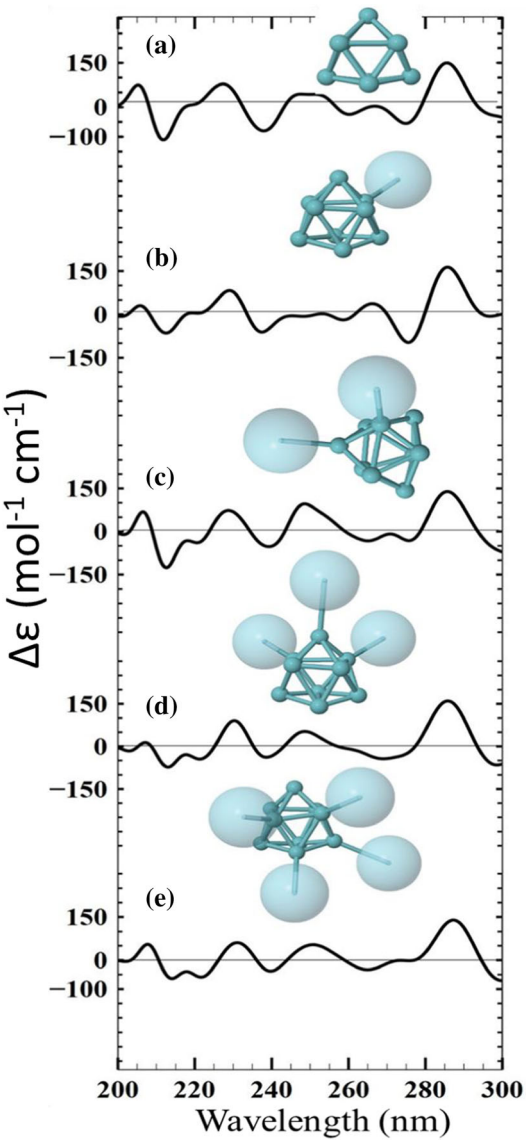

Fig. 7 Simulated ECD spectra for Nb_9Ar_n clusters shown in the second row of Fig. 1 ($\sigma = 0.2$ eV)

able to assume the iso1/iso2 coexistence in real samples, underlying the importance of isomerization effects as already suggested by Fielicke et al. [29].

In Figs. 2, 3 and 4, we now plot the UV–Vis spectra in the 200–1000 nm range for all our considered Nb_9Ar_n ($n = 0$–4) complexes to evaluate if the different cluster geometries presented in Fig. 1 are spectroscopically distinguishable. The simulated spectra shown in Figs. 2b–e, 3b–e, and 4b–e correspond to the argon-containing Nb_9 clusters presented in Figs. 1a–d, e–h, and i–l, respectively, also shown as insets in the figures. Finally, the data plotted in Figs. 2a, 3a, and 4a were obtained from the bare iso1, iso2, and iso3 structures, respectively. In all cases, a broad absorption spectrum is found [we use a full width at half maximum (FWHM) equal to 3000 cm^{-1}], characterized by a main absorption band located at ~ 240 nm, where a complex mixture of multiple electronic excitations originates the formation of this maxima. For example, as a representative case, the excitation located at 240.4 nm in Fig. 2e is composed of the following electronic transitions between occupied (HOMO-i) and virtual (LUMO-j) molecular orbitals [where their participation (in %) is indicated in parenthesis]: H-19 → L + 21 (2%), H-19 → L + 24 (7%), H-12 → L + 28 (7%), H-3 → L + 40 (2%), H-21 → L + 10 (7%), H-20 → L + 20 (2%), H-19 → L + 21 (2%), H-19 → L + 22 (4%), H-11 → L + 29 (4%), H-9 → L + 30 (5%). Similarly, in Fig. 3e the excitation placed at 242.1 nm is composed of the following electronic transitions: H-22 → L + 11 (3%), H-17 → L + 25 (2%), H-17 → L + 26 (2%), H-15 → L + 27 (2%), H-12 → L + 26 (2%), H-11 → L + 29 (2%), H-7 → L+31 (4%), H-6 → L+32 (2%), H-6 → L+34 (4%), H-19 → L+23 (2%), H-18 → L+25 (8%), H-17 → L+25 (2%), H-15 → L + 28 (2%). As expected, low-lying and high-lying states are involved in these electronic transitions, being thus of fundamental importance to per-

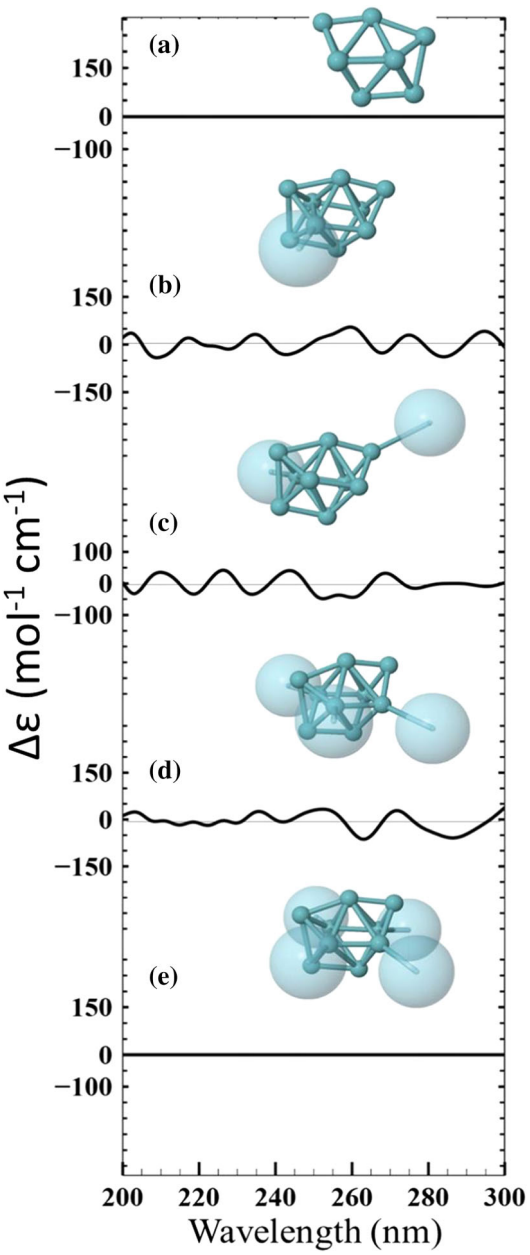

Fig. 8 Simulated ECD spectra for Nb_9Ar_n clusters shown in the third row of Fig. 1 ($\sigma = 0.2$ eV)

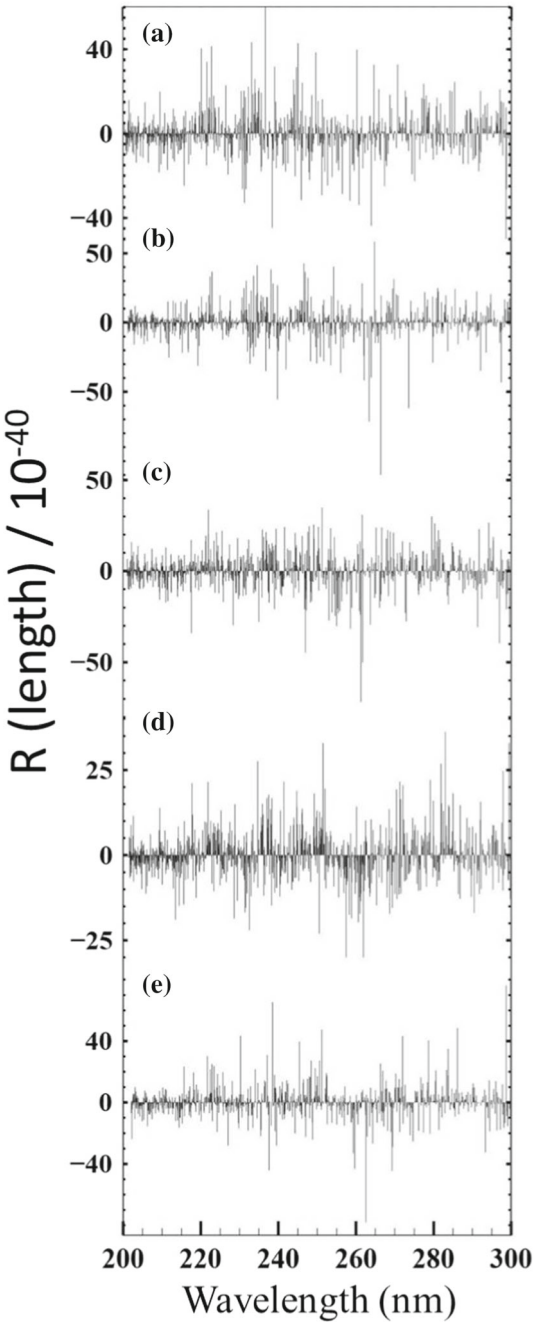

Fig. 9 Simulated rotational strength R (in 10^{-40} esu^2 cm^2) in the 200–300 nm range corresponding to the Nb_9Ar_n clusters ($n = 0$–4) shown in Fig. 6

form an accurate description of the orbital energies in this wavelength range. Finally, we notice from Figs. 2, 3 and 4 the existence of less intense absorption bands in the range of 300–400 nm together with a vanishing optical response near the visible part of the spectra.

We must emphasize that our simulated UV–Vis spectra are in qualitative agreement with the experimental measurements of Warren et al. [56] who reported the optical absorption spectra of Nb_nAr clusters with $n = 7$–20 atoms in the 336–634 nm range. In the particular case of the Nb_9Ar complex, the use of photodissociation spectroscopy reveals the onset of the UV–Vis response at $\sim$ 600 nm in agreement with our theoretical calculations plotted in Figs. 2b, 3b, and 4b. However, in the measured data we also appreciate fine details in the spectra such as the existence of well-defined bands at approximately 400, 500, and 580 nm. In order to evaluate if our TD-DFT calculations are able to reproduce these specific details of the experimental curve we plot in Fig. 5 the discrete distribution of electronic transitions as a function of their oscillator strength underlying the spectra plotted in Figs. 2b, 3b, and 4b. From Fig. 5, we actually note, for our three-

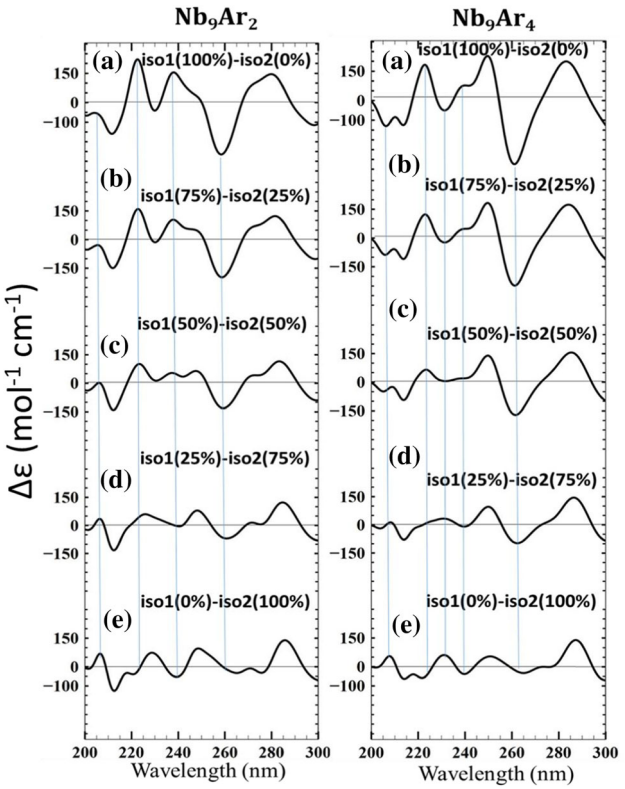

Fig. 10 Calculated weighted averages of the ECD spectra obtained for the two lowest energy Nb_9Ar_2 isomers shown in Figs. 6c and 7c (left column) as well as for Nb_9Ar_4 complexes presented in Figs. 6e and 7e (right column) ($\sigma = 0.2$ eV)

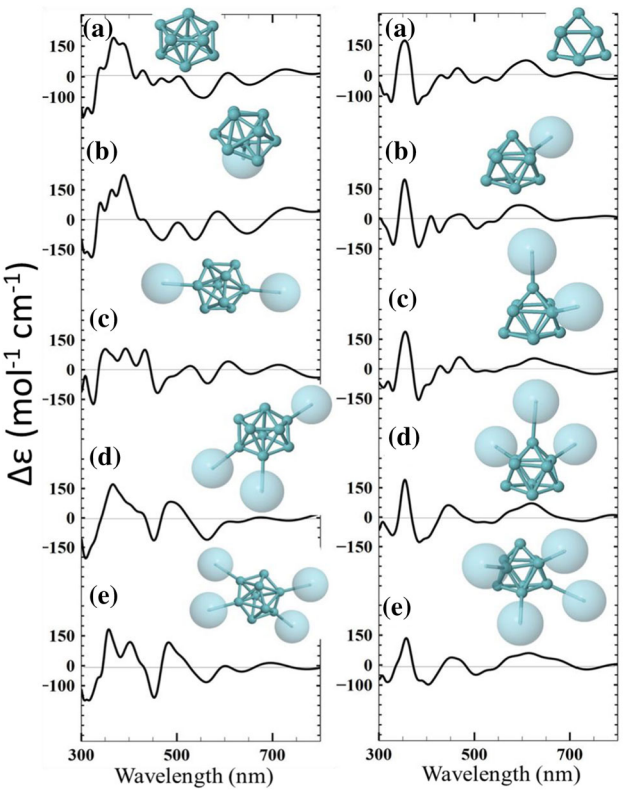

Fig. 11 Simulated ECD spectra for Nb_9Ar_n clusters shown in the first (left column) and second (right column) rows of Fig. 1 in the 300–800 nm range ($\sigma = 0.2$ eV)

considered Nb_9Ar clusters, the existence of high densities of electronic transitions around 400, 500, and 580 nm (being most notable in Fig. 5b) in qualitative agreement with the experimental observations, a fact that give us confidence in the accuracy of our theoretical description. Interestingly, the authors of Ref. [56] compare their experimental spectra for the Nb_9Ar complex with the one measured by Collings et al. [57] on Nb_9Kr clusters and found that they look very similar, although the Nb_9Ar cluster exhibits more intense absorption bands. The authors attribute these variations to systematic differences in pump laser fluency normalization procedures between the two experiments. In this sense, we have run some test calculations on Nb_9Kr clusters to obtain their absorption spectra (see Fig. S4 of the supporting information) and found that the presence of single Kr or Ar atoms on the surface of all three iso1, iso2, and iso3 Nb_9 isomers leaves the UV–Vis spectra practically unchanged underlying, as stated in Ref. [56], the importance of the experimental conditions employed to measure the electronic excitations. In general, the shape of all the measured spectra looks very similar, defining thus UV–Vis spectroscopy as not very appropriate to identify the geometrical structure of small Nb clusters.

In Figs. 6, 7 and 8, we now plot the simulated ECD spectra in the experimentally accessible 200–300 nm range for all our considered isomers shown in Fig. 1 (using a bandwidth $\sigma = 0.2$ eV). The calculated spectra reported in Figs. 6b–e, 7b–e, and 8b–e correspond to the argon-containing Nb_9 clusters presented in Fig. 1a–d, e–h, and i–l, respectively, also shown as insets in the figures. Finally, the data plotted in Figs. 6a, 7a, and 8a were obtained from the bare iso1, iso2, and iso3 structures, respectively. From Figs. 6, 7 and 8, we observe that the ECD signals of Nb_9Ar_n complexes strongly depend on the local atomic environment. While, as shown in Fig. 6, the non-planar hexagonal structures reveal both intense and broad CD bands, negligible and not very informative signals are found in Fig. 8 for distorted triply capped octahedral clusters presented as insets in the figure. In contrast, Nb_9Ar_n complexes where Nb atoms are arranged in a triply capped trigonal prism (Fig. 7) reveal a notable distribution of positive and negative bands, although with reduced intensities. In each figure, when varying the number of surrounding Ar atoms, no significant spectral shifts are found; however, we do observe appreciable variations in the relative intensity between some neighboring CD signals, mainly in the 200–260 nm range. Interestingly, when moving from 3 to 4 adsorbed argons, negligible changes in the shape and intensity of the Cotton bands are observed all along the ECD spectra.

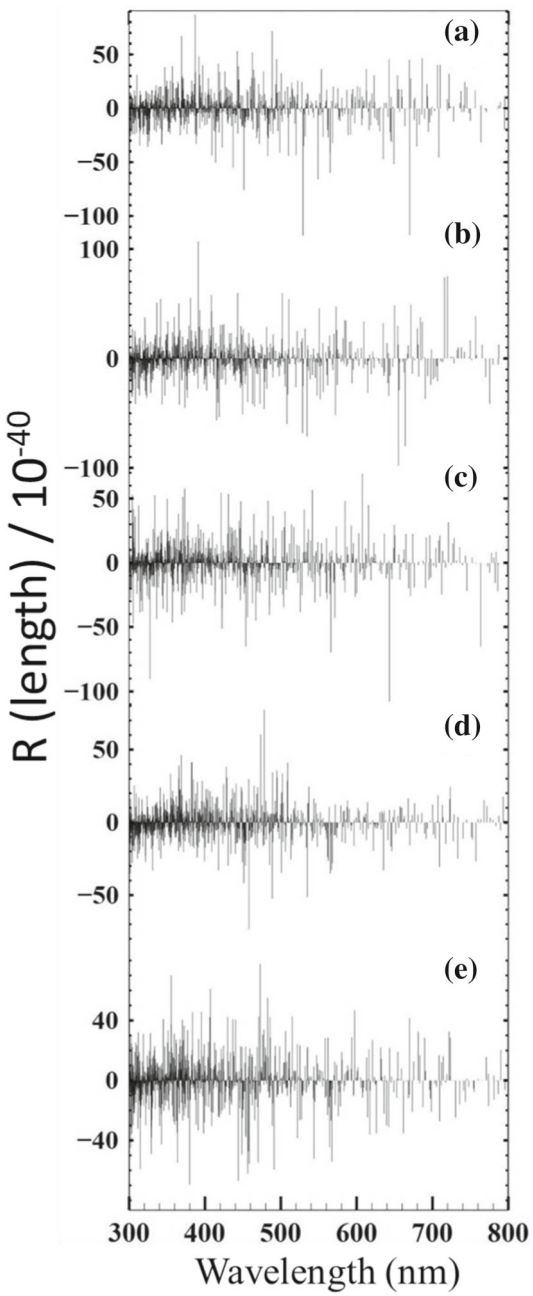

Fig. 12 Simulated rotational strength R (in 10^{-40} esu^2 cm^2) in the 300–800 nm range corresponding to the Nb_9Ar_n clusters (n = 0–4) shown in Fig. 11-left

Based on the results plotted in Figs. 6, 7 and 8, we can state that our simulated ECD spectra show precise features that allows us to clearly distinguish between different 9-atom Nb cluster isomers. In particular, the highly covered Nb_9Ar_4 structure shown in Fig. 6e is characterized by three well-defined positive bands located at 221, 249, and 282 nm, together with a profound minima placed at 261 nm, which are spectral features being unique to the highly covered argon-containing iso1 structures. Notice that the existence of CD bands at 221 and 260 nm are also observed in the bare cluster case which in conjunction with the rest of the signals are expected to be of fundamental importance for absolute configurational determination in the gas phase. We must emphasize that, in general, the location of the maxima and minima in the ECD spectra shown in Figs. 6 and 7 correlates well with the maxima and minima obtained in the corresponding absorption spectra presented in Figs. 2 and 3. This is clearly illustrated in Figs. S5 and S6 of the supporting information where, as representative examples, we compare UV–Vis and ECD data for the iso1 bare and Nb_9Ar_4 structures, respectively. We must emphasize that the well-defined optical activity observed in some Nb_9 clusters is also relevant for biological systems where chirality-dependent sensing and catalytic reactions typically occur.

Besides the existence of well-defined CD bands in Nb_9Ar_n clusters (n = 0–4) shown in the previous figures it is also important to analyze the magnitude of our predicted rotational strengths R in order to evaluate if the Cotton signals are large enough to be experimentally determined. In Fig. 9, we show, as representative examples, the R-value distribution for the iso1 Nb_9Ar_n (n = 0–4) complexes shown in Fig. 6 which exhibit the most notable CD bands. From Fig. 9a–e, we notice, in the 200–300 nm domain, a complex distribution of positive and negative values for R with intensities varying in the range of – 100 to 70. We also observe that local distributions of excitations determine the shape of the ECD curve. For example, in Fig. 9a, the large number of positive excitations (66) which lie between 215 and 228 nm leads to the formation of a positive CD band observed in Fig. 6a. Similarly, in the 245–275 nm domain, there exist a majority of negative and intense excitations (110) that originate the well-defined minima obtained in Fig. 6a centered at 260 nm. Additional features can be also understood by these local distributions for the R values like for example the disappearance (appearance) of the CD band located at 235 nm (250 nm) when moving from Fig. 6a–e. In that case, the 15 positive excitations obtained in Fig. 9a around 235 are reduced to 11 in Fig. 9e, having in addition associated intensities diminished by 73%. In contrast, in the 240–250 nm range, we note that 51 positive excitations are developed upon argon complexation of the Nb_9 cluster surface, a fact that leads to the appearance of a well-defined CD band at 250 nm. We must say that, at the moment, there are no experimental measurements of the ECD spectra or optical rotation on gas-phase niobium clusters to compare our R values and more precisely evaluate the reliability of our TD-DFT calculations.

Our results presented in the previous figures predict the existence of the Cotton effect in Nb_9Ar_n clusters. However, we must emphasize that our calculations have been performed for isolated niobium clusters in vacuum, whereas in situations that are more realistic solvent effects as well as the presence of multiple isomers might play an important role in the interpretation of the experimental data. This last case is important to analyze since the measured spectra will be thus the result

of a complex average of the optical behavior of different cluster conformations. In addition, and in contrast to infrared spectroscopy, the existence of positive and negative CD bands as shown in Figs. 6, 7 and 8 will play a fundamental role since, upon averaging, both cancellation and signal enhancements might occur. Consequently, an interesting improvement in our calculations could be achieved by computing weighted averages of the ECD spectra for the highly stable argon-containing iso1 and iso2 clusters shown in Figs. 6 and 7, in order to gain insight into the changes that might occur in the distribution of CD bands due to the coexistence of different structures.

In Fig. 10, we plot, as representative examples, different weighted averages of the ECD spectra shown in Figs. 6c and 7c (left column of Fig. 10) as well as in Figs. 6e and 7e (right column of Fig. 10). The previous averages correspond to the optical properties of the low-energy isomers shown in Figs. 1b, f as well as in Fig. 1d, h. Notice from Fig. 10b-left that if a small amount of the iso2 Nb_9Ar_2 structure is considered (25%), a sizable reduction in the intensity of the CD bands, when compared to Fig. 10a-left, is already observed. However, when the iso1(50%)–iso2(50%) case is analyzed (Fig. 10c-left), a notable transformation of the ECD spectra is found. The pronounced two-peak structure observed in Fig. 10a-left within the 220–250 nm range is transformed into three well-defined bands with reduced intensities located at 222, 237, and 248 nm (Fig. 10c-left). Interestingly, when the iso2 isomer is the dominant species (Fig. 10d-left), the average spectrum is strongly perturbed since we now observe two separated peaks placed at 225 and 248 nm, as well as a new positive CD band that emerges at 208 nm which is absent in Fig. 10a-left. Similar spectral changes are found in Fig. 10-right when averaging the optical properties of Nb_9Ar_4 iso1 and iso2 cluster structures, namely *i*) a strong dependence of the ECD spectra on the relative amount of the considered isomers, (*ii*) a sizable quenching in the intensity of CD bands, and (*iii*) the appearance and/or disappearance of Cotton signals all along the spectra. According to our calculations, a zero value in the ECD spectra in real samples could indicate, on the one hand, that right and left circularly polarized light is equally adsorbed by the argon-containing clusters and, on the other hand, even if individual Nb clusters are chiral, an ensemble of these objects may produce the absence of the Cotton effect due to cancellation effects.

We would like to point out that, in the case of iso1 and iso2 structures, the development of CD signals extending near the infrared region of the spectra has been found. This is clearly observed from Fig. 11 where we plot, in the 300–800 nm domain, the ECD bands of all Nb_9Ar_n iso1 (left column) and iso2 (right column) clusters shown in the first and second rows of Fig. 1, respectively. Notice that, in the 300–500 nm range, the signals for the highly stable Ar-containing iso1 complexes shown in Fig. 11-left reveal a distribution of sharp positive and negative Cotton bands whose intensity and location, in contrast to the data plotted in Fig. 6, are more sensitive to the number of adsorbed Ar species. Interestingly, this is not the case for the iso2 Nb_9Ar_n clusters presented in Fig. 11-right where an isolated and pronounced peak placed at approximately 350 nm is always observed, a signal that can be used to identify the presence of iso2 structures in a sample. However, despite the spectral differences between the two isomers shown in the previous figure, negligible CD lines are found in both cases for wavelengths larger than 700 nm. These results reveal that cluster identification could be also achieved from various regions of the ECD spectra since different isomer-specific signals can be found.

Finally, in Fig. 12 we show, as a representative case, the simulated rotational strength R in the 300–800 nm range associated to the ECD spectra of Nb_9Ar_n clusters ($n = 0$–4) plotted in Fig. 11-left. As already obtained from Fig. 9 we appreciate from Fig. 12 (i) a complex distribution of positive and negative values for R all along the here-considered nanometer range, (ii) local densities of excitations in specific domains that determine the shape of the CD bands, and (iii) magnitudes of R varying in the range of $-$ 110 to 100 which we believe could lead to their spectroscopic characterization. Interestingly, above 650 nm, we note in general an almost equal distribution in the number, intensity, as well as in the amount of positive and negative signs for the values of R that leads to a cancellation of the ECD curve near the visible part of the spectra.

4 Summary and conclusions

In this work, we have presented the first time-dependent density functional theory investigation dedicated to analyze the electronic circular dichroism of Nb_9Ar_n ($n = 0$–4) clusters. The ECD spectra reveal a strong dependence of the distribution of Cotton bands to the local atomic environment where, in contrast to infrared spectroscopy, not only the location and intensity but also the sing of the Cotton signals shows significant variations for different Nb_9 isomers. The calculated values for the rotatory strengths seem to be large enough to be experimentally determined. The comparison of the here-reported theoretical predictions with gas phase CD measurements will be thus of fundamental important to identify the presence of specific clusters in a sample. Actually, by performing different weighted averages of ECD spectra corresponding to our two more stable isomers we have found significant variations in the Cotton bands, being strongly dependent on the relative amount of the coexisting species, and underlying the importance of isomerization effects. Based on the previous results we speculate that, in real samples, a zero value in the ECD spectra could indicate that right and left circularly polarized light is equally adsorbed by the argon-containing clusters or that, even if individual Nb clusters are chiral, an ensemble of these objects may produce the absence of the Cotton effect due to cancellation effects. Finally, we also observe the existence

of CD bands in the 300–700 nm region of the spectra showing a higher sensitivity to the cluster geometry and to the number of surrounding argon atoms. We hope that the here-reported TF-DFT predictions will motivate additional theoretical studies with a higher degree of accuracy, as well as experiments addressing both gas phase and solution CD measurements in these kind of systems.

4.1 Supplementary material

See the supplementary material for additional UV–Vis and ECD spectra as well as new data involving the calculation of the density of states for the studied Nb clusters.

Acknowledgements The authors would like to acknowledge the financial support from Consejo Nacional de Ciencia y Tecnología (CONACyT), México. Computer resources from the ACARUS supercomputer center from the Universidad de Sonora, México, as well as from the Laboratorio Nacional de Supercómputo del Sureste (LNS), México, are also acknowledged.

Author contributions

This research was planned by RAG, and DCN-I calculations were performed by DCN-I. The two authors discussed the results. RAG-L wrote the manuscript.

Data Availability Statement This manuscript has data included as electronic supplementary material.

References

1. P. Jena, Q. Sun, Super atomic clusters: design rules and potential for building blocks of materials. Chem. Rev. **118**, 5755–5870 (2018)
2. X. Wang, Z. Cao, X. Lu, M. Lin, Q. Zhang, Structure and stability of binary transition-metal clusters $(NbCo)_n$ ($n \leq 5$): a relativistic density-functional study. J. Chem. Phys. **123**, 064315 (2005)
3. M.D. Morse, Clusters of transition-metal atoms. Chem. Rev. **86**, 1049–1109 (1986a)
4. H. Arslan, M.H. Guven, Melting dynamics and isomer distributions of small metal clusters. New J. Phys. **7**, 60 (2005)
5. B. Anak, M. Bencharif, F. Rabilloud, Time-dependent density functional study of UV–Visible absorption spectra of small noble metal clusters (Cu_n, Ag_n, Au_n, n = 2-9, 20). RCS Adv. **4**, 13001–13011 (2014)
6. T.M. Soini, N. Rosch, Size-dependent properties of transition metal clusters: from molecules to crystals and surfaces—computational studies with the program ParaGauss. Phys. Chem. Chem. Phys. **17**, 28463–28483 (2015)
7. P. Ranjan, T. Chakraborty, Structure and electronic properties of Au_nPt (n = 1-8) nanoalloy clusters: the density functional theory study. J. Nanopart. Res. **22**, 35 (2020)
8. A. Bérces, P.A. Hackett, L. Lian, S.A. Mitchell, D.M. Rayner, Reactivity of niobium clusters with nitrogen and deuterium. J. Chem. Phys. **108**, 5476–5490 (1998)
9. V.J.F. Lapoutre, M. Haertelt, G. Meijer, A. Fielicke, J.M. Bakker, IR spectroscopy of neutral transition metal clusters through thermionic emission. J. Chem. Phys. **139**, 121101 (2013)
10. M. Haertelt, V.J.F. Lapoutre, J.M. Bakker, B. Redlich, D.J. Harding, A. Fielicke, G. Meijer, Structure determination of anionic metal clusters via infrared resonance enhanced multiple photon electron detachment spectroscopy. J. Phys. Chem. Lett. **2**, 1720–1724 (2011)
11. M.B. Knickelbein, Reactions of transition metal clusters with small molecules. Ann. Rev. Phys. Chem. **50**, 79–115 (1999)
12. B.F.G. Johnson, J.S. McIndoe, Spectroscopic and mass spectrometric methods for the characterization of metal clusters. Coord. Chem. Rev. **200–202**, 901–932 (2000)
13. H. Kietzmann, J. Morenzin, P.S. Bechthold, G. Gantefor, W. Eberhardt, D.S. Yang, P.A. Hackett, R. Fournier, T. Pang, C. Chen, Photoelectron spectra and geometric structures of small nioubium cluster anions. Phys. Rev. Lett. **77**, 4528–4531 (1996)
14. J. Conceicao, R.T. Laaksonen, L.-S. Wang, T. Guo, P. Nordlander, R.E. Smalley, Photoelectron spectroscopy of transition-metal clusters: correlation of valence electronic structure to reactivity. Phys. Rev. B **51**, 4668 (1995)
15. K. Koyasu, J. Atobe, S. Furuse, A. Nakajima, Anion photoelectron spectroscopy of transition metal- and lanthanide metal-silicon clusters: MSi_n − (n =6–20). J. Chem. Phys. **129**, 214301 (2008)
16. K. Ohshimo, T. Komukai, T. Takahashi, N. Norimasa, J.W.J. Wu, R. Moriyama, K. Koyasu, F. Misaizu, Application of ion mobility-mass spectrometry to the study of ionic clusters: investigation of cluster ions with stable sizes and compositions. Mass Spectrom. **3**, S0043 (2014)
17. M.J. Manard, P.R. Kemper, Characterizing the electronic states of the second-row transition metal cations using high-resolution ion mobility mass spectrometry. Int. J. Mass Spec. **407**, 69–76 (2016)
18. T. Masubuchi, J.F. Eckhard, K. Lange, B. Visser, M. Tschurl, U. Heiz, An efficient laser vaporization source for chemically modified metal clusters characterized by thermodynamics and kinetics. Rev. Sci. Instrum. **89**, 023104 (2018)
19. U. Heiz, E.L. Bullock, Fundamental aspects of catalysis on supported metal clusters. J. Mater. Chem. **14**, 564–577 (2004)
20. M.R. Zakin, R.O. Brickman, D.M. Cox, A. Kaldor, Dependence of metal cluster reaction kinetics on charge state. I. Reaction of neutral (Nb_x) and ionic (Nb_x^+, Nb_x^-) niobium clusters with D_2. J. Chem. Phys. **88**, 3555 (1988)
21. T.C. Hung, T.W. Liao, Z.H. Liao, P.W. Hsu, P.Y. Cai, W.H. Lu, J.H. Wang, M.F. Luo, Dependence on size of supported Rh nanoclusters for CO adsorption. RSC Adv. **6**, 3830–3839 (2016)
22. S.M. Lang, I. Fleischer, T.M. Bernhardt, R.N. Barnett, U. Landman, Low-temperature CO oxidation catalyzed by free palladium clusters: similarities and differences

to pd surfaces and supported particles. ACS Catal. **5**, 2275–2289 (2015)
23. M. Maier-Borst, D.B. Cameron, M. Rokni, J.H. Parks, Electron diffraction of trapped cluster ions. Phys. Rev. A **59**, R3162 (1999)
24. A. Lechtken, C. Neiss, M.M. Kappesab, D. Schooss, Structure determination of gold clusters by trapped ion electron diffraction: $Au_{14^-} - Au_{19^-}$. Phys. Chem. Chem. Phys. **11**, 4344–4350 (2009)
25. J.C. Rivoal, C. Grisolia, J. Lignieres, D. Kreisle, P. Fayet, L. Wöste, Absorption spectroscopy of size-selected trimers and pentamers transition metal clusters isolated in rare gas solids: preliminary steps. Zeitschrift für Physik D Atoms Mol. Clust. **12**, 481–484 (1989)
26. M.D. Morse, Clusters of transition metal atoms. Chem. Rev. **86**, 1049–1109 (1986b)
27. S. Yang, M.B. Knickelbein, Photoionization studies of transition metal clusters: Ionization potentials for Fe_n and Co_n. J. Chem. Phys. **93**, 1533 (1990)
28. M.W. Rossa, A.W. Castleman, Ultrafast ionization and subsequent coulomb explosion of zirconium oxide and tungsten carbide "superatomic" cluster species and comparison to group 10 metals. New J. Chem. **36**, 2253–2259 (2012)
29. A. Fielicke, C. Ratsch, G. von Helden, G. Meijer, Isomer selective infrared spectroscopy of neutral metal clusters. J. Chem. Phys. **122**, 091105 (2005)
30. A.-M. Valente-Feliciano, Superconducting RF materials other than bulk niobium: a review. Supercond. Sci. Technol. **29**, 113002 (2016)
31. T. Tsuchida, Y. Azuma, Synthesis of niobium carbide and nitride in air from mechanically activated Nb–C powder mixtures. J. Mater. Chem. **7**, 2265–2268 (1997)
32. I. Nowak, M. Ziolek, Niobium compounds: preparation, characterization, and application in heterogeneous catalysis. Chem. Rev. **99**, 3603–3624 (1999)
33. P.V. Nhat, M.T. Nguyen, Structures, spectra, and energies of niobium clusters from Nb_{13} to Nb_{20}. J. Phys. Chem. A **116**, 7405–7418 (2012)
34. D. Masuzaki, T. Nagata, F. Mafuné, Desorption of oxygen from cationic niobium oxide clusters revealed by gas phase thermal desorption spectrometry and density functional theory calculations. J. Phys. Chem. A **121**, 2079–2085 (2017)
35. F.N.N. Pansini, M. de Campos, A.C. Neto, C.S. Sergio, Chem. Phys. **535**, 110778 (2020)
36. W. Ma, L. Xu, A.F. de Moura, X. Wu, H. Kuang, C. Xu, N.A. Kotov, Chiral inorganic nanostructures. Chem. Rev. **117**, 8041–8093 (2017)
37. J.M. Solar, M.A. Ozkan, H. Isci, R. Mason, Electronic absorption and magnetic circular dichroism spectra of some planar platinum(II), palladium(II), and nickel(II) complexes with phosphorus-donor ligands. Inorg. Chem. **23**, 758–764 (1984)
38. J. Autschbach, F.E. Jorge, T. Ziegler, Density functional calculations on electronic circular dichroism spectra of chiral transition metal complexes. Inorg. Chem. **42**, 2867–2877 (2003)
39. M. Arai, W. Kosaka, T. Matsuda, S.I. Ohkhosi, Observation of an iron(II) spin-crossover in an iron octacyanoniobate-based magnet. Ang. Chem. **47**, 6885–6887 (2008)
40. D.J. Robbins, A.J. Thomson, Magnetic circular dichroism spectra of the octahedral niobium and tantalum subhalide clusters $[M_6X_{12}]^{n+}$. J. Chem. Soc. Dalton Trans. **21**, 2350–2364 (1972)
41. C.S. Lehmann, N.B. Ram, I. Powis, M.H.M. Janssen, Imaging photoelectron circular dichroism of chiral molecules by femtosecond multiphoton coincidence detection. J. Chem. Phys. **139**, 234307 (2013)
42. M. Pitzer, How to determine the handedness of single molecules using Coulomb explosion imaging? J. Phys. B At. Mol. Opt. Phys. **50**, 153001 (2017)
43. T. Kitamura, T. Nishide, H. Shiromaru, Y. Achiba, N. Kobayashi, Direct observation of "dynamic" chirality by Coulomb explosion imaging. J. Chem. Phys. **115**, 5 (2001)
44. L. Satterthwaite, C. Pérez, A.L. Steber, D. Finestone, R.L. Broadrup, D. Patterson, Enantiomeric analysis of chiral isotopomers via microwave three-wave mixing. J. Phys. Chem. A **123**, 3194–3198 (2019)
45. M.J. Frisch, G.W. Trucks, H.B. Schlegel, G.E. Scuseria, M.A. Robb, J.R. Cheeseman, G. Scalmani, V. Barone, B. Mennucci, G.A. Petersson, H. Nakatsuji, M. Caricato, X. Li, H.P. Hratchian, A.F. Izmaylov, J. Bloino, G. Zheng, J.L. Sonnenberg, M. Hada, M. Ehara, K. Toyota, R. Fukuda, J. Hasegawa, M. Ishida, T. Nakajima, Y. Honda, O. Kitao, H. Nakai, T. Vreven, J.A. Montgomery Jr., J.E. Peralta, F. Ogliaro, M.J. Bearpark, J. Heyd, E.N. Brothers, K.N. Kudin, V.N. Staroverov, R. Kobayashi, J. Normand, K. Raghavachari, A.P. Rendell, J.C. Burant, S.S. Iyengar, J. Tomasi, M. Cossi, N. Rega, N.J. Millam, M. Klene, J.E. Knox, J.B. Cross, V. Bakken, C. Adamo, J. Jaramillo, R. Gomperts, R.E. Stratmann, O. Yazyev, A.J. Austin, R. Cammi, C. Pomelli, J.W. Ochterski, R.L. Martin, K. Morokuma, V.G. Zakrzewski, G.A. Voth, P. Salvador, J.J. Dannenberg, S. Dapprich, A.D. Daniels, Ö. Farkas, J.B. Foresman, J.V. Ortiz, J. Cioslowski, D.J. Fox, *Gaussian 09* (Gaussian Inc., Wallingford, 2009)
46. Y. Wang, X. Jin, H.S. Yu, D.G. Truhlar, X. He, Revised M06-L functional for improved accuracy on chemical reaction barrier heights, noncovalent interactions, and solid-state physics. PNAS **114**, 8487–8492 (2017)
47. N. Godbout, D.R. Salahub, J. Andzelm, E. Wimmer, Optimization of Gaussian-type basis sets for local spin density functional calculations. Part I. Boron through neon, optimization technique and validation. Can. J. Chem. **70**, 560–571 (1992)
48. F. Weigend, R. Ahlrichs, Balanced basis sets of split valence, triple zeta valence and quadruple zeta valence quality for H to Rn: Design and assessment of accuracy. Phys. Chem. Chem. Phys. **7**, 3297–3305 (2005)
49. E.G. Lewars, *The Concept of the Potential Energy Surface. Computational Chemistry*, 2nd edn. (Springer, Dordrecht, 2011)
50. P.J. Stephens, N. Harada, ECD Cotton effect approximated by the Gaussian curve and other methods. Chirality **22**, 229–233 (2010)
51. A.K. James, P. Kowalczyk, R. Fournier, B. Simard, J. Chem. Phys. **99**, 8504 (1993)
52. D.A. Hales, L. Lian, P.B. Armentrout, Int. J. Mass. Spectrom. Ion Proc. **102**, 269 (1990)
53. M.B. Knickelbein, S. Yang, J. Chem. Phys. **93**, 1476 (1990)

54. H. Wang, R. Craig, H. Haouari, Y. Liu, J.R. Lombardi, D.M. Lindsay, J. Chem. Phys. **105**, 5355 (1996)
55. T. Pradeep, B. Niu, D.A. Shirley, Photoelectron spectroscopy of rare gas dimers revisited: vibrationally resolved photoelectron spectrum of argon dimer. J. Chem. Phys. **98**, 5269–5275 (1993)
56. W.J.C. Menezes, M.B. Knickelbein, J. Chem. Phys. **98**, 1856–1866 (1993)
57. B.A. Collings, K. Athanassenas, D.M. Rayner, P.A. Hackett, Zeitschrift für Physik D Atoms Mol. Clust. **26**, 36–40 (1993)